Phase behavior and molecular interactions in mixtures of ceramide with dipalmitoylphosphatidylcholine

Dolores C. Carrer and Bruno Maggio[1]

Departamento de Química Biológica-CIQUIBIC, Facultad de Ciencias Químicas-CONICET, Universidad Nacional de Córdoba, Ciudad Universitaria, 5000 Córdoba, Argentina

Abstract **In mixtures with dipalmitoylphosphatidylcholine, ceramide induces broadening of the calorimetric main phase transition that could be deconvoluted into at least three components: the first represents isothermal melting of a phosphatidylcholine-enriched phase; the second and third represent phases with increasing proportions of ceramide melting at progressively higher temperatures. The partial phase diagram (up to 40 mole % ceramide) indicates complete or partial gel-phase immiscibility, and complete gel- and liquid-phase miscibility depending on the ceramide content. Cluster distribution function analysis of each individual transition reveals decreased cooperativity and domain size with increased amounts of ceramide. Compared to individual lipids, mixed monolayers with dipalmitoylphosphatidylcholine show unchanged mean molecular areas or slight expansions at 24°C with dipole potentials exhibiting hyperpolarization; by contrast, already at 27°C the mean molecular areas become condensed and dipole potentials show little changes or are slightly depolarized. This suggests that favorable ceramide–phosphatidylcholine dipolar matching in the liquid state can be one of the local determinants for close molecular interactions while unfavorable matching may explain lateral domain segregation of ceramide-enriched gel phases. The changes are detected at relatively low proportions of Cer (1–12 mole %) which are comparable to variations of Cer levels in membranes of cultured cells undergoing functional responses mediated by the sphingomyelin signaling pathway.**—Carrer, D. C., and B. Maggio. **Phase behavior and molecular interactions in mixtures of ceramide with dipalmitoylphosphatidylcholine.** ***J. Lipid Res.*** **1999.** 40: **1978–1989.**

Supplementary key words calorimetry • monolayers • ceramide • phase diagram

Biological membranes contain a rich variety of lipids and, besides the relatively stable pools of major and minor lipid classes, other components are formed in transient amounts during various cellular processes (1–4). Several of these transient lipids such as diacylglycerols, fatty acids, and lysoderivatives accomplish major roles as second messengers in different membrane-associated transduction pathways that are mediated by phospholipases acting on specific glycerophospholipids. These lipid messengers can cause major alterations of the membrane structure and dynamics (5–8) and their catalytic formation is selectively regulated by the membrane organization and composition (9–11).

On the other hand, the degradation of sphingomyelin constitutes another important membrane transduction pathway involving a production of ceramide (Cer) that can be triggered by several stimuli in a variety of cellular effects (3, 4). Cer is also the initial and final step for the biosynthesis and degradation of complex glycosphingolipids that are present in relatively small amounts in membranes (12). These lipids are important biomodulators of membrane function (13) and induce dramatic and amplified perturbations of the bilayer properties in terms of lipid–lipid and lipid–protein interactions (14), phase state (15), surface electrostatics (14, 16), non-bilayer phases and topology (17, 18), membrane–membrane interactions (19), and interfacial modulation of various phosphohydrolytic enzymes (20, 21). Thus, Cer is a central structural and functional component in the metabolic pathway of several classes of sphingolipids. Due to this pivotal metabolic position, Cer can be an efficient effector and signal amplifier molecule responding to a variety of membrane-mediated cellular functions that are initiated or regulated through the participation of many different sphingolipids

In addition, it has been recently shown that both sphingomyelin and glycerophospholipid degradation pathways mediated by sphingomyelinase and phospholipase A_2, which are key elements of lipid-mediated signaling, can be mutually modulated at the interfacial level by the presence of substrates and products formed by both catalytic reactions (22). The activity of both phosphohydrolytic

Abbreviations: Cer, ceramide (N-acyl sphingoid); dpPC, 1,2-dihexadecanoyl-*sn*-glycero-phosphocholine; dmPC, 1,2-ditetradecanoyl-*sn*-glycero-phosphocholine; dePE, dielaidoylphosphatidylethanolamine; ΔC_{pmax}, maximum excess heat capacity; ΔH_{cal}, calorimetric enthalpy; T_m, temperature corresponding to ΔC_{pmax}; ΔH_{VH}, van't Hoff enthalpy; T_S, onset temperature for melting; T_L, final temperature for melting; $\Delta V/n$, surface potential per unit of molecular surface density; ΔG_{excess}, excess free energy of mixing.

[1] To whom correspondence should be addressed.

pathways, as selectively regulated by their non-common intermediates, can lead to amplification or damping of the transduction reactions at the membrane interface depending on the lateral surface pressure and composition (23).

In spite of the emergence of Cer as a key component for the cross-modulation of glycero- and sphingo-phospholipid degradative pathways (3, 4, 22, 23), scarce information is as yet available on its effects on the molecular organization of well-defined model membrane systems which should, in the end, be at the basis of its functional role. The variety of components present in cellular membranes and the complex structural dynamics of cellular systems preclude detailed investigations of the possible changes induced by Cer because, at the molecular level, the studies require precisely controlled conditions. A few reports in recent years have shown that Cer perturbs the structure of phosphatidylcholine bilayers in different ways depending on the relative proportions of both lipids and on the type of fatty acid amide-linked to the sphingosine moiety (24). Also, the enzymatic degradation of sphingomyelin and phosphatidylcholine to Cer and diacylglycerol by the combined action of sphingomyelinase and phospholipase C induces structural changes of lipid bilayers leading to membrane fusion (7) and it has been demonstrated that Cer facilitates formation of non-bilayer phases although less effectively than diglyceride (25).

Concentration of Cer in defined membrane domains can be of importance for biological response amplification or induction of signaling cascades and for modifying membrane structure and metabolism. In the present work we studied in detail the molecular determinants of the effects induced by Cer on the organization of dipalmitoylphosphatidylcholine (dpPC) at the thermodynamic, dipolar, and molecular packing levels using high sensitivity differential scanning calorimetry, cluster distribution function analysis, and lipid monolayers.

MATERIALS AND METHODS

Materials

Bovine brain ceramide (type III) from Sigma-Aldrich Inc. (St. Louis, MO), contains primarily stearic (18:0) (31.6% w/w) and nervonic (15-tetracosenoic) (48% w/w) fatty acids and was over 99% pure according to HPTLC developed in Cl_3CH:MetOH:H_2O (26).

Dipalmitoylphosphatidylcholine was from Avanti Polar Lipids (Alabaster, AL). Water was double distilled in an all glass apparatus. Solvents were of the highest purity available from Merck (Darmstadt, Germany).

Calorimetry

Lipids were premixed in the desired proportions from solutions prepared in chloroform–methanol 2:1. The mixture was taken to dryness as a thin film in a conical-bottom tube under a stream of N_2 and submitted to vacuum for at least 4 h. The dry lipid was hydrated (at a final concentration between 2.5–3.5 mm) with double-distilled water by freeze–thaw cycling at least five times between −70°C and 90°C; multilamellar dispersions were formed by vigorous vortexing above 70°C. The dispersion of vesicles was introduced, after degassing under reduced pressure, into the sample cell of a MC2D-Microcal high sensitivity differential scanning calorimeter (Microcal Inc., Amherst, MA) with the reference cell filled with double-distilled water. The proportions of Cer with respect to dpPC varied between 0–40 mole % and the total amount of dpPC was kept between 1.8 and 2.3 mg/ml in the calorimeter cell while the amount of total lipid varied accordingly. Samples were scanned at 45°C/h and triplicate runs were performed with different vesicle loads; the scans were fully reproducible after cooling to 15°C and immediate reheating. The transitions were normalized, averaged, analyzed, and deconvoluted with the software provided with the instrument and with the PeakFit program from Jandel Scientific (San Rafael, CA). For DSC thermograms showing complex excess heat capacity profiles, suggesting more than one underlying transition, the curves were resolved mathematically into the number of necessary peaks, assuming independent transitions, so that the sum of these constituents gave the best fit to the original data. After this, cluster distribution functions were calculated following the method of Freire and Biltonen (27) for each of the previously resolved peaks.

Lipid monolayers

Monolayers were spread from premixed solutions of the lipids in chloroform–methanol 2:1. Details of the equipment used were given in previous publications (21, 22). Surface pressure isotherms and surface potential isotherms versus molecular area were obtained at the indicated temperature by spreading less than 15 μl of lipid solution on the surface of double-distilled water contained in one of the compartments (90 cm^2) of a specially designed circular Teflon-coated trough of a Monofilmmeter (Mayer Feintechnik, Germany) with a platinized-Pt sensing plate connected to a surface pressure transducer; surface potential was measured by a high impedance millivoltmeter (Corning ionalyzer 250) connected to a surface ionizing electrode formed by an ^{241}Am plate positioned 5 mm above the monolayer surface, and to a reference calomel electrode connected to the aqueous subphase through a saline bridge. Temperature was maintained within ±0.3°C with a refrigerated Haake F3C thermocirculator. At least duplicate monolayer isotherms were obtained and averaged at a compression rate of 0.45–0.60 $nm^2 \cdot molecule^{-1} \cdot min^{-1}$; reducing the compression speed further produced no change in the isotherms. Reproducibility was within maximum SEM of ±1 mN/m for surface pressure, ±20 mV for surface potential, and ±0.02 nm^2 for molecular areas. Absence of surface-active impurities in the subphase and in the spreading solvents was routinely controlled as described (21). The excess free energy of mixing was calculated as the difference between the area under the experimental and the ideal surface pressure–molecular area isotherms, integrated between 1 mN/m and the film's collapse pressure (28).

RESULTS AND DISCUSSION

Thermotropic mesomorphism

Figure 1A shows representative actual scans of excess heat capacity as a function of temperature for pure dpPC and mixtures with Cer in different proportions. Cer is very difficult to hydrate (29, 30) and does not form well-dispersed mesophases in excess water that can be homogeneously introduced into the calorimetric cell for liquid samples available in our DSC instrument. Similar to other glycosphingolipids (29), by repeated cycling between very

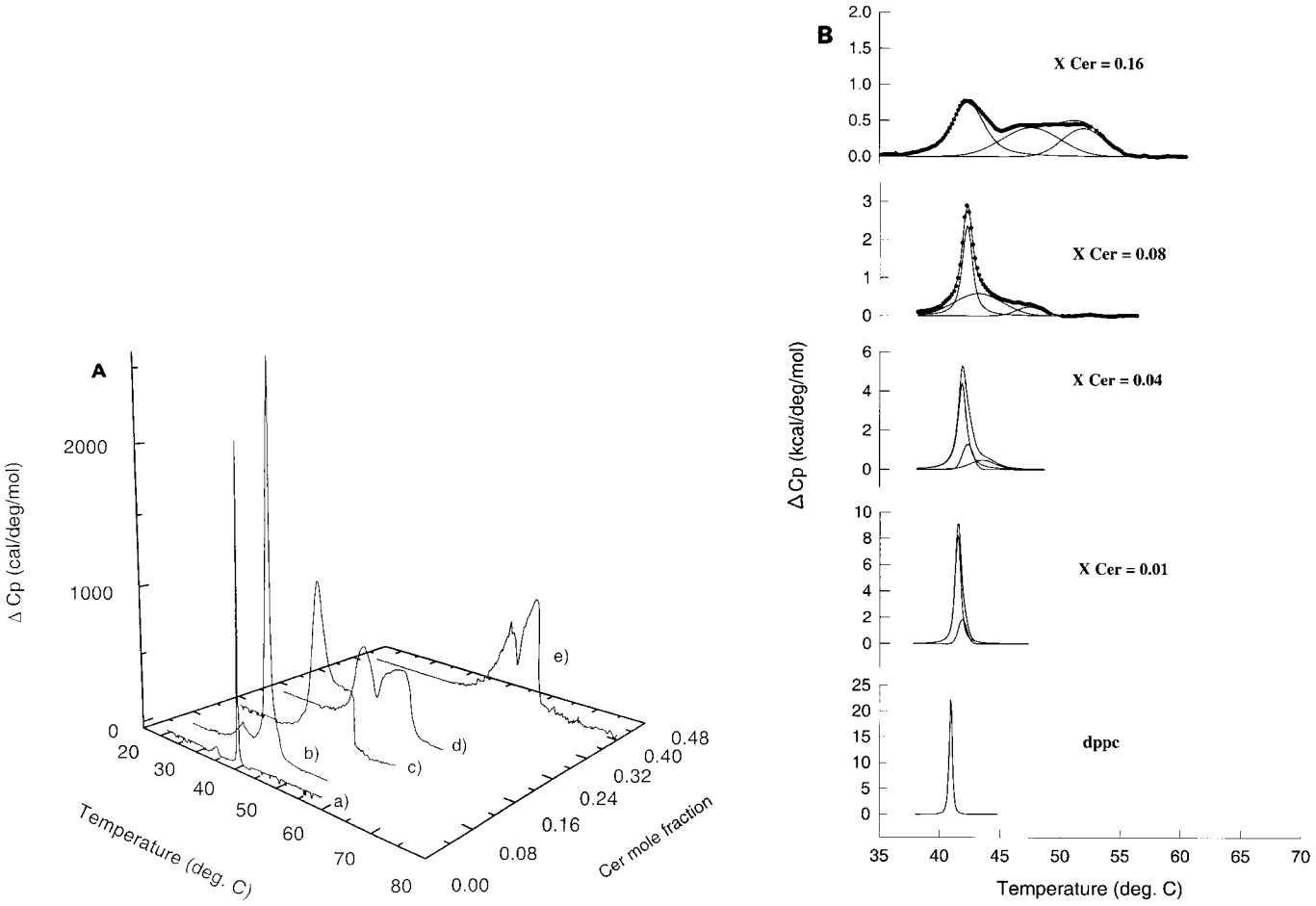

Fig. 1. High sensitivity differential scanning calorimetry of mixtures of Cer with dpPC. A) Calorimetric raw data of representative samples containing dpPC (a); 4% Cer (b); 12% Cer (c); 20% Cer (d); 40% Cer (e). The ordinate values for curves (a) and (b) were multiplied by 0.1 and 0.5, respectively. B) Peaks deconvoluted from the calorimetric data of representative mixtures. Calorimetric raw data (●) are shown for comparison in the curves for samples with 8 and 16 mole % Cer.

low and high temperatures (above 90°C) we were able to produce homogeneous aqueous dispersions, with reproducible thermotropic behavior, of mixtures containing Cer up to 40 mole %, but above this proportion Cer prevented proper hydration and homogeneous dispersion of the sample. From studies in monolayers at different temperatures it was previously inferred that Cer should undergo a bulk phase transition temperature above 80°C (31), but the monolayer data do not allow to establish cooperativity. We could not detect any cooperative phase transition of our pure Cer sample in excess of water (below 0.23% w/v lipid), scanned at 45°C/h, over the range of 2–110°C. In dry and partially hydrated samples (and thus quite concentrated in terms of lipid mass) of different species of Cer scanned at a relatively rapid scan rate of 5°C/min, both reversible and metastable endothermic transitions occurred in the 70–100°C range; the position of the peaks varied with the amount of water in the system and depended on the presence and type of hydroxylated fatty acyl chain amide-linked to the sphingosine moiety (32, 33). The latter also influence the intermolecular packing arrangement of ceramides in monolayers at the air-water interface (34).

The presence of Cer at only 1 mole % in the mixture with dpPC induces a decrease of the ΔC_{pmax}, an 8% reduction of the total ΔH_{cal}, a broadening of the pretransition (not shown, but see Fig. 1A for 4 mole % Cer), and a high temperature asymmetry of the main transition peak (Fig. 1B). The broadening of the pretransition is accompanied by a gradual increase of its T_m; at 8 mole % Cer, the latter has risen by 1°C and the pretransition peak begins to overlap with the main transition. At 12 mole % Cer, the pretransition is no longer distinguishable. The van't Hoff thermodynamic cooperative unit [$\Delta H_{VH}/\Delta H_{cal}$ (35)] of the main phase transition shows a decrease of about 33% compared to pure dpPC (from 250 molecules in pure dpPC to 166 molecules in the mixture). The asymmetry toward the high temperature side induced by Cer at 1 mole % is the consequence of a small additional transition peak centered at 41.7°C. This second transition becomes clearly evident in mixtures containing more than 2 mole % Cer (see for example curve for 4 mole % Cer in Fig. 1B). The asymmetry indicates a preferential partition of Cer in the liquid–crystalline phase of dpPC compared to the gel phase. The asymmetric distortion of the excess heath capacity versus temperature function increases progres-

sively with the proportion of Cer and becomes a well-distinguished shoulder in mixtures containing 8 mole % Cer (Fig. 1B). In these mixtures ΔC_{pmax} has fallen by about 87% compared to pure dpPC. At over 12 mole % Cer, the endothermic phase change spans a wide temperature range (15 to 20°C) and all the deconvoluted transitions reveal rather small cooperative units (below 110 molecules).

The calorimetric data are summarized in **Fig. 2** as a partial temperature–composition phase diagram showing the variation of the onset and completion temperatures, and the T_m of each deconvoluted transition. The new transition maxima, induced by increasing proportions of Cer, occur at progressively higher temperatures (Fig. 2) and their coexistence with lower-melting components reflect the presence of phase separated domains. The general tendency is that each new higher-melting transition coexists with at least one transition of lower T_m that was already present in mixtures containing a lower proportion of Cer.

The phase diagram clearly indicates that the onset temperature at which the gel phase starts to melt (T_S) remains practically constant up to a mole fraction of Cer of 0.08. The isothermal onset melting temperature of the gel phase, independent on the proportion of Cer in that range of composition, means that Cer is immiscible with and does not become incorporated into the gel phase lattice of dpPC. At a mole fraction of Cer of 0.12, the sphingolipid becomes partially miscible with dpPC in the gel phase as indicated by the decrease of T_S by more than 2°C. Then, T_S remains again essentially constant and independent on the proportion of Cer up to a mole fraction of the latter of 0.3. The fact that T_S of the mixture is lower than that of pure dpPC and constant over this range of composition indicates the melting of a defined solid solution (partial miscibility) containing a constant amount of Cer (between 8–12 mole %). Between a mole fraction of 0.3 and 0.4, the onset temperature shows an abrupt rise (11°C); this represents the point at which the mixed dpPC-Cer gel phase containing 8–12 mole % Cer ceases to be present and transforms into a new gel-phase more enriched in Cer. The mixture of dpPC with 8–12 mole % Cer represents a distinct gel phase (S_2) that forms over this composition range and that is immiscible with both the perturbed dpPC gel phase (S_1) and with the higher-melting phase (S_3) representing the mixture most enriched in Cer. On the other hand, the phase diagram clearly indicates that the completion temperature (T_L) increases gradually with the proportion of Cer from the beginning (see inset in Fig. 2) reflecting the preferential miscibility of Cer with the liquid–crystalline phase of dpPC at any proportion of Cer.

The peak of the first deconvoluted transition (peak 1) progressively shifts its position upwards, moving from 40.9°C (pure dpPC) to 43°C at a mole fraction of Cer of 0.3, while decreasing its contribution to the total ΔH_{cal} of the transition (**Fig. 3**); this transition is no longer detectable in the mixture containing 40 mole % Cer. The decrease of ΔH_{cal} of peak 1 takes place in two clear steps: a steep decline from the value of pure dpPC to that corresponding to a mole fraction of Cer of 0.08, a plateau in mixtures containing mole fractions of Cer from 0.12 to 0.20, and a final decrease of ΔH_{cal} until peak 1 disappears in the mixture with a mole fraction of Cer of 0.4. The phase with the T_m corresponding to peak 2 can be already detected in the mixture with 1 mole % Cer and its ΔH_{cal} increases by

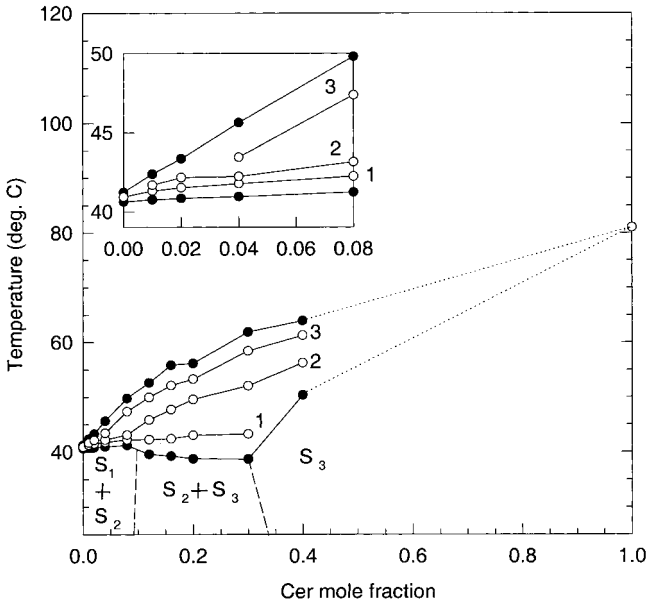

Fig. 2. Partial calorimetric phase diagram for the dpPC-Cer system. The numbers on the curves refer to the peaks characterizing the first, second, and third constitutive transitions. Open symbols are T_m values and closed symbols are onset and completion temperatures. The inset shows an enlarged view of the calorimetric behavior of mixtures containing up to 8 mole % Cer. An indicative T_m for pure Cer is marked at 81°C (see text).

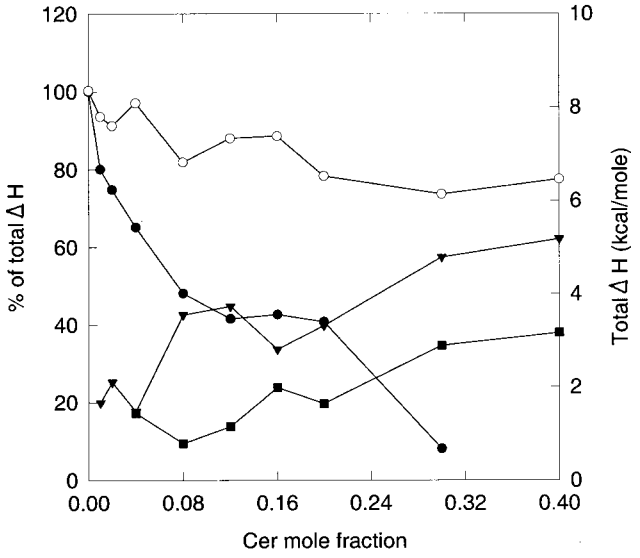

Fig. 3. Calorimetric enthalpies of individual transitions of mixtures of Cer and dpPC. Variation of total ΔH_{cal} (○) and of the contribution to total ΔH_{cal} of peak 1 (●); peak 2 (▼); and peak 3 (■) with the amount of Cer in the mixture. The ΔH_{cal} of pure dpPC corresponds to 8.6 Kcal/mole. Maximum SEM were below ± 10% of the values shown.

about 100% when the mole fraction of Cer changes from 0.04 to 0.08; subsequently it remains approximately constant for mixtures containing between 12 and 20 mole % Cer, increasing again its contribution to the total ΔH_{cal} for systems containing a mole fraction of Cer between 0.2–0.4 (Fig. 3). The third deconvoluted transition (peak 3) can already be detected at 4 mole % Cer; it is always the smaller peak and increases its ΔH_{cal} and the contribution to the total transition enthalpy very gradually (Fig. 3).

Up to 8 mole % Cer peak 1 probably corresponds to the melting of phase S1 mostly constituted by laterally segregated dpPC that is increasingly perturbed by the incorporation of a small amount of Cer. From the decrease of ΔH_{cal} of the transition corresponding to peak 1 (phase S_1 in this range of concentration of Cer) it can be calculated (15) that an average of about 14 molecules of dpPC per molecule of Cer are prevented from undergoing their own phase transition. Between mole fractions of Cer of 0.08 to 0.20, the plateau in ΔH_{cal} of peak 1 coincides with the region at which the T_m of this peak remains approximately constant (shifted by about 1.3°C upward from pure dpPC, see Fig. 2). In this part of the phase diagram, the proportion of Cer in the first melting phase represented by peak 1 is locked at the point where the "solidus" line T_S in the phase diagram shifts by about 2°C downwards, representing the melting of a phase S2, containing 8–12 mole % Cer. Over this range of composition disappearance of phase S1 occurs with formation of a new gel phase S3. In the range of mole fraction of Cer between 0.08 and 0.3, peak 2 probably represents the melting of phase S3. The approximately constant values of ΔH_{cal} of peaks 1 and 2 further indicates that these phases coexist, with their intermolecular interactions rather unperturbed by each other's presence, over a mole fraction of Cer between 0.12 and 0.2. However, the amount of energy required to dissociate molecular interactions in order to transform the gel lattice into the liquid–crystalline state increases continuously with the proportions of Cer. In fact, the second and third deconvoluted transitions (peaks 2 and 3) shift the position of their T_ms towards higher temperatures as the proportion of Cer increases. Peak 3 probably represents the melting of a gel phase highly enriched in Cer that exists only at temperatures at which most of the dpPC in the system is already in the liquid–crystalline state with which Cer is preferably miscible.

Cluster domain distributions

The transition properties of the lipid phase have their origin in the changes of the configurational state of the lipid molecules which, in turn, affects their intermolecular organization, miscibility, and topographical distribution of coexisting phase domains in the two-dimensional plane. The thermodynamic parameters corresponding to the calorimetrically determined excess heat capacity–temperature function reflect the variation of the size and number of coexisting gel and liquid crystalline cluster domains that are in dynamic equilibrium during the phase transition (27, 36). For some lipid systems the latter has been successfully interpreted on molecular terms assuming statistical thermodynamic models for the hydrocarbon chain configuration as a function of the thermal energy available (37–39). In more complex systems statistical thermodynamic modeling is limited because several contributions to the partition function are unknown or their estimation is uncertain. We have analyzed the behavior of our dpPC-Cer system with an operational alternative treatment (27, 36) that can directly obtain the partition function from experimental excess heat capacity–temperature functions that have been previously deconvoluted into single peak constitutive transitions. This approach, previously applied to a pure phospholipid and binary mixtures with hydrophobic molecules (27) and a few glycolipids (14), permits the calculation of thermodynamic cluster domain averages and surface densities, gel–liquid crystalline fractional boundaries, and probability distribution functions and fluctuations underlying each individual transition without requiring the assumption of a molecular configuration model for the phase transition. Obviously, any inference about detailed local molecular configuration is lost and the various distribution and size functions correspond only to thermodynamically correlated molecular changes that may not have a direct topographical correlate. The results can be interpreted and discussed only within this context.

The peaks obtained from deconvolution analysis of the calorimetrically determined excess heat capacity–temperature function assuming two-state independent phase transitions are always symmetric and $T_m = T_{1/2}$. Due to this, a same average number of lipid molecules are thermodynamically correlated (average cluster size) in the gel and liquid crystalline phases at the T_m. **Figure 4** shows that for each deconvoluted peak the properties of the most probable cluster at the corresponding T_m are a function of the proportion of Cer in the mixture. This indicates that, similar to other binary mixtures containing lipid-perturbing agents (27), the thermodynamic changes induced by Cer on the phase transition properties reflect altered underlying molecular distribution effects.

The variation of the average size of the thermodynamic clusters is in keeping with the changes of the cooperative unit calculated as the ratio $\Delta H_{VH}/\Delta H_{cal}$. Figure 4A shows that the size of the most probable cluster at the T_m of the deconvoluted transitions corresponding to peaks 1, 2, and 3 shows a marked decrease when the amount of Cer in the system exceeds 8 mole %. The average cluster size at the T_m of peak 1, which represents the phase most enriched in dpPC (phase S_1), decreases to about half the size of the average cluster of pure dpPC with only 2 mole % Cer and remains at approximately similar low values up to a mole fraction of Cer of 0.08; with increased proportions of Cer the cluster size decreases again to a very small number of molecules before the transition represented by peak 1 is abolished above 30 mole % Cer (phase S_2). The transition defined by peak 2 is characterized by relatively large cluster sizes at the T_m in systems containing between 1 and 4 mole % Cer; the cluster size at the T_m of this transition decreases to very small values in systems with a mole fraction of Cer of 0.08 or above (phase S_3). The higher-

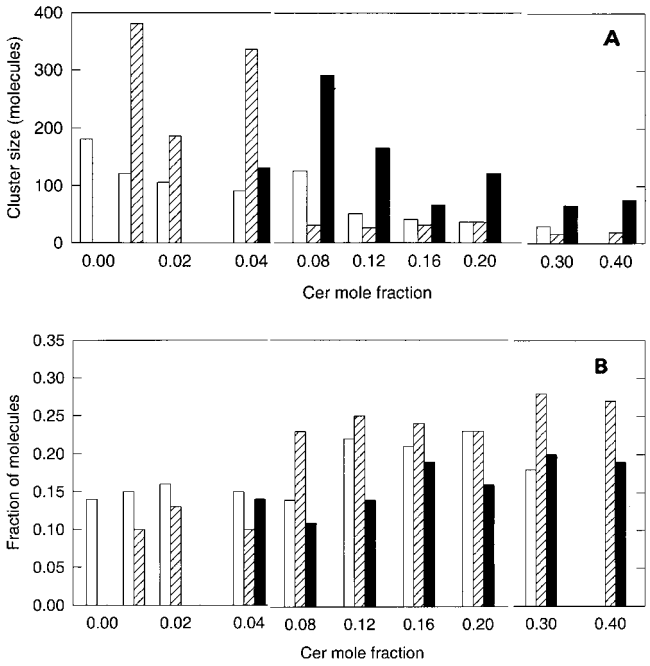

Fig. 4. Cluster parameters of the deconvoluted transitions. The size of the most probable cluster at T_m (A), and the fraction of molecules in the gel–liquid boundaries at T_m (B) are shown for the transitions represented by peak 1 (solid white), peak 2 (cross-hatched), and peak 3 (solid black).

melting transition characterized by peak 3 represents the phase most enriched in Cer. The size of the most probable cluster at the T_m of this component transition reaches a maximum at about 8 mole % Cer and decreases gradually thereafter. It should be emphasized that the statistical thermodynamic analysis is performed on each previously deconvoluted transition. Therefore, the alteration of the cluster distribution properties of each defined segregated domain by the presence of another phase with a different proportion of Cer also indicates that these phases coexist within a same supramolecular structural lattice that is modified by Cer in the long range.

Overall, Cer appears to induce a dispersion of clusters of reduced size in the segregated phase least enriched in Cer while causing a relative increase of the domain size in the Cer-enriched phase. Subsequently, when the proportion of Cer is increased in the system, new phases more enriched in Cer are formed and the variation of the domain pattern is repeated. The average cluster densities (not shown) also indicate the trend described but in a reverse manner, reflecting the logic that large cluster densities reflect relatively small average cluster size and vice versa. A similar but more "buffered" variation pattern is found for the fraction of molecules at the gel–liquid crystalline boundary (Fig. 4B); it should be noted that for several systems the average size of the cluster domains causes a considerable proportion of lipids to reside at the cluster boundaries and are thus likely to experience lateral intermolecular packing defects. Marked increases of this boundary lipid fraction occur when the system contains between 8 and 12 mole % Cer.

The average cluster sizes corresponding to the constitutive transitions of the mixtures containing different proportions of Cer are thermodynamic entities characterized by large fluctuations (27). The relative probability that a lipid molecule resides in a gel (or liquid–crystalline) cluster of a defined size at the T_m has a rather broad distribution with a large average fluctuation whose magnitude is approximately equal to the average cluster size itself. The cluster distribution function is different depending on the proportion of Cer: in general, as the amount of Cer increases and the size of the most probable cluster diminishes, the probability distribution of domain sizes becomes sharper. This is illustrated in **Fig. 5** for peak 1.

Molecular interactions in lipid monolayers

Calorimetry can efficiently describe the thermodynamic features of the phase transition and miscibility properties of mixtures of dpPC and Cer but the molecular details of intermolecular packing are not directly accessible with this technique. We therefore used mixed lipid monolayers to investigate the effects of Cer on the intermolecular packing, surface pressure-induced two-dimensional transitions and dipolar interactions in the mixed films with dpPC.

Cer forms a liquid-condensed film at 24°C with a limiting mean molecular area of 0.40 nm^2 and surface potential of 515 mV at the collapse pressure of 40 mN/m (40), the maximum compressibility modulus of 205 reflects a rather condensed state above surface pressures of 5 mN/m and mean molecular areas below 0.45 nm^2 (41). The surface pressure–area isotherms of the mixtures with dpPC in different proportions show ideal behavior or small positive deviations at 24°C depending on the surface pressure

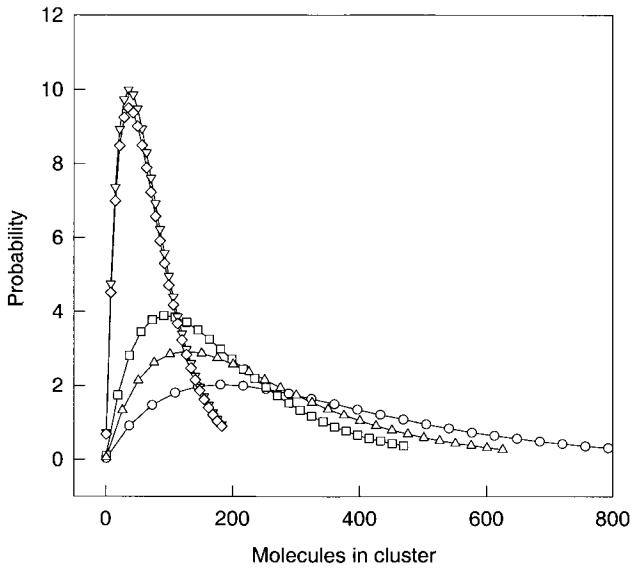

Fig. 5. Probability distribution function of cluster sizes of the dpPC-enriched phase. The probability that a molecule of the transition represented by peak 1 resides in a gel cluster formed by the number of molecules indicated in the abscissa is shown for mixtures of pure dpPC (○), and mixtures containing Cer at 4 mole % (□), 8 mole % (△), 20 mole % (▽), and 30 mole % (◇).

(**Fig. 6B**) which means that the individual components undergo negligible variation or slight expansion (below 10%) of their individual mean molecular area in the mixture. Because of its marked dependence on the lateral surface pressure, isothermal two-dimensional phase transitions in monomolecular films are very sensitive to small changes in temperature (31). Compared to the bulk phase behavior described above, mixed films of the Cer–dpPC show that marked differences of the two-dimensional behavior are induced by relatively small temperature changes. The inset in Fig. 6A shows that an increase in temperature to 27°C already causes a change in the interactions. At this temperature mixtures with a mole fraction of Cer between 0.05 and 0.8 exhibit negative deviations from the ideal behavior at surface pressures below 16 mN/m (that is when the monolayer is in the liquid-expanded state), and essentially ideal behavior in the condensed state at high surface pressures. Also, the two-dimensional surface pressure-induced transition of dpPC is no longer detectable at 27°C in mixtures with a mole fraction of Cer of 0.14 even if a mixed film exhibiting ideal mixing behavior should clearly reveal it (Fig. 6A). At the lower temperature of 24°C, an increased mole fraction of Cer of 0.4 is needed to abolish the phase transition.

The values of the compressibility modulus (41) and its variations as a function of the mean molecular packing areas reflect precisely both the physical state of the monolayer film and the presence of two-dimensional transitions (**Fig. 7**). The compressibility modulus, which gives a quantitative measure of the state of the monolayer, is obtained directly from the slope of the pressure–area curve as $K = -(A\,\delta\Pi/\delta A)_T$. For a gaseous monolayer the compressibility modulus is numerically similar to the figure for the surface pressure; for liquid states it varies between 12.5 and 250, and for solids between 1000 and 2000 (41). Thus, a defined minimum or abrupt variation of the slope of the curve of compressibility modulus versus area indicates with high sensitivity the occurrence of a change in the physical state of the monolayer, for example the coexistence of expanded-condensed phase transitions in the film.

Monolayers of pure dpPC show a defined beginning (at 0.85 nm^2) and end (at 0.6 nm^2) of the liquid-expanded to liquid-condensed transition and a relatively smooth conversion to increasingly condensed states as the surface pressure is increased; this corresponds to the typical behavior of a diffuse first-order transition in which both phases coexist over a certain range of surface pressures and mean molecular areas (31, 42). The two-dimensional phase transition is clearly indicated by the change of the surface compressibility modulus over this range of molecular packing areas (Fig. 7A). In mixed

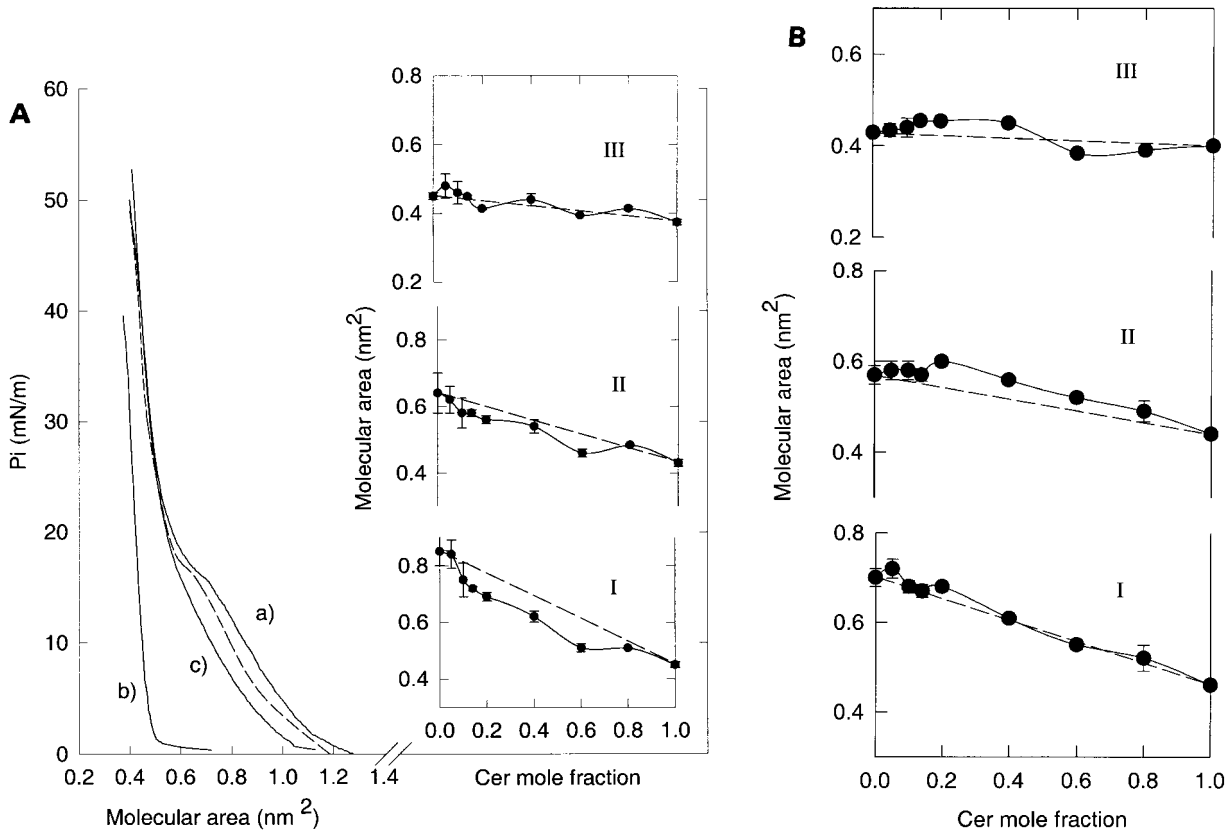

Fig. 6. Molecular area vs. surface pressure. (A) Typical lateral pressure–molecular area isotherms at 27°C for pure dpPC (a), pure Cer (b), a mixture containing 14 mole % Cer (c), and the calculated isotherm for the ideal mixture with 14 mole % Cer (dashed line). The inset shows variation of molecular area with the mole fraction of Cer at 27°C at lateral pressures of I) 10 mN/m, II) 17 mN/m, III) 39 mN/m. (B) Variation of molecular area with the mole fraction of Cer at 24°C at lateral pressures of I) 10 mN/m, II) 15 mN/m, III) 40 mN/m.

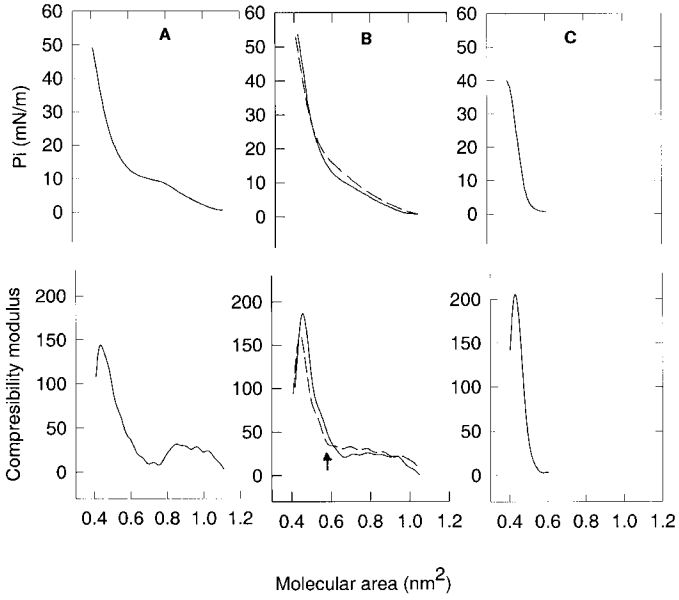

Fig. 7. Surface pressure– and surface compressibility modulus–molecular area isotherms. The variations of surface pressure (upper panels) and surface compressibility modulus (lower pannels) with the mean molecular area are shown at 24°C for pure dpPC (A), a mixture with a mole fraction of Cer of 0.14 (B), and pure Cer (C). For comparison, the dashed line in (B) shows the data at 27°C. The arrow indicates the abrupt phase transition point (see text).

films containing more than 10 mole % Cer at 27°C, the surface pressure–molecular area isotherm no longer shows the two-dimensional phase transition (see Fig. 7B, dashed line), while this is still evident at 24°C (Fig 7B, solid line). However, the variation of the compressibility modulus is a more sensitive parameter to detect the state of the film and indicates the existence of an abrupt liquid-expanded–liquid-condensed transition for mixtures containing a mole fraction of Cer of 0.14, 0.2, and 0.4 at 27°C. This is illustrated in Fig. 7B for a mole fraction of Cer of 0.14 (dashed line). The phase transition is not readily observable in the pressure–area curve, but the compressibility modulus shows at 0.6 nm^2 (arrow) a clear conversion from a state of constant compressibility in the range of values of liquid-expanded monolayers to a state of increasing condensation. This type of transition is different from that occurring in pure dpPC and the range of molecular packing and surface pressure over which the condensed and expanded states coexist is extremely small (which makes it practically undetectable in the surface pressure–molecular area isotherm). In these interfaces the condensed and expanded phases cannot coexist in a mixed lattice under compression and become mutually excluded in the lateral plane; this appears to correspond to a better defined abrupt first-order class resembling the highly cooperative discontinuous transitions observed for monolayer phase states of some fatty acids (42).

As shown in the two-dimensional surface pressure–composition isothermal phase diagram at 24°C (**Fig. 8B**), the transition from the liquid-expanded to the liquid-condensed state of dpPC remains isobaric independent of the proportions of Cer until it is no longer detectable at a mole fraction of Cer of 0.4. This indicates poor interaction of Cer with dpPC at this temperature, in agreement with the near ideal behavior or slight expansions followed by the variation of mean molecular area as a function of composition in the mixed films. At 27°C, 5 mole % Cer induces a decrease of 4 mN/m in the lateral surface pressure for the transition onset which remains at 12 ± 1 mN/m in the mixture with 10 mole % Cer and becomes undetectable at 14 mole % Cer. The fact that the isothermal phase transition disappears at smaller amounts of Cer when the temperature is increased to 27°C indicates the enhanced interaction of Cer with liquid-expanded dpPC.

In spite of being uncharged, Cer causes marked changes of the dipole potential in the mixed films with dpPC. This is similar to the changes in surface potential reported for mixtures of dpPC with mono- and diglyceride lipids having the hydroxyl moiety in their polar head group and indicates that charge–dipole and dipole–dipole interactions occur between both lipids (14, 43). These affect both the magnitude and the orientation of the resultant perpendicular molecular dipole moments depending on intermolecular packing. **Figure 9** shows the surface potential per unit of molecular surface density (usually denominated surface potential/molecule). At 24°C the deviations from ideality of this parameter are positive at mole fractions of Cer between 0.14 and 0.6, indicating that the average overall film dipoles are hyperpolarized compared to mixtures with no interactions (Fig. 9A). This is well correlated to the expansions of molecular area observed at this temperature (Fig. 6B). Again, the relatively small increase of temperature to 27°C causes a marked difference in the dipolar interactions. As can be seen, at 27°C the deviations from ideal behavior are negative at a surface pressure of 15 mN/m and mole fractions of Cer below 0.2 (Fig. 9B) and at 5 mN/m in the range of mole fractions of Cer of 0.1 to 0.6; this indicates favorable dipolar matching occurring with interfacial depolarization together with increased interaction and reductions of the mean molecular areas com-

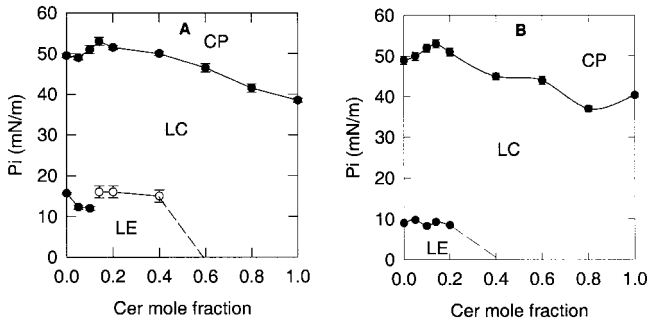

Fig. 8. Two-dimensional phase diagrams summarizing the monolayer data obtained at 27°C (A) and at 24°C (B). CP, collapsed phase; LC, liquid condensed phase; LE, liquid expanded phase. In (A), the open symbols represent the pressure points at which an abrupt change in compressibility modulus of the type shown in Fig. 7B is observed.

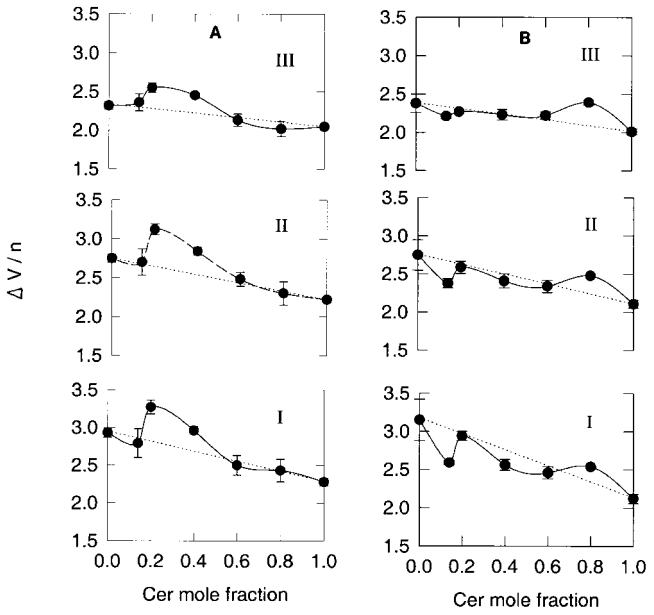

Fig. 9. Variation of surface potential per unit of molecular surface density ($\Delta V/n$) with the mole fraction of Cer. The results are shown at 24°C (A) for surface pressures of (I) 5 mN/m; (II) 9 mN/m; (III) 30 mN/m or at 27°C (B) for surface pressures of (I) 5 mN/m; (II) 15 mN/m; (III) 30 mN/m.

pared to ideal films (see Fig. 6A). The deviations of the surface potential/molecule become positive in films highly enriched in Cer (mole fraction of 0.8) again indicating unfavorable dipolar hyperpolarization probably leading to apparent ideal mixing behavior of the mean molecular area as a function of composition. This is in keeping with induction of lateral segregation of domains enriched in Cer as indicated by the calorimetry studies. As deduced from cluster distribution function analysis, these domains should be smaller in size due to unfavorable dipolar matching.

At 24°C the excess free energy of mixing ΔG_{excess} shows small values all below absolute figures of about 90 cal/mole. On the basis of the reproducibility of the surface pressure–molecular area isotherms stated in the Materials and Methods section values of ΔG_{excess} (which are obtained from the integrated area under the isotherm) below this figure cannot be considered significant. Operationally this means that these mixtures appear as ideal or slightly unfavorable at 24°C from the point of view of the two-dimensional work necessary to pack them in the monolayer arrangement from 1 mN/m up to the collapse pressure. At 27°C ΔG_{excess} varies between −90 and −200 cal/mol. This again indicates that the interactions of dpPC with Cer in practically all proportions are thermodynamically favored at 27°C.

CONCLUSIONS AND IMPLICATIONS

Interpretation in molecular terms of the multiple cellular effects mediated by endogenous or exogenous Cer, such as in cell growth, differentiation and apoptosis, under the influence of a large variety of stimuli is not readily accomplished because of the lack of precise molecular control over the complex cellular systems in which those biological effects are observed. In addition, in many studies of the cellular effects, compounds analogous to Cer are frequently used because of the inherent difficulties involved in dispersing natural Cer in aqueous solutions (such as fluorescent and very short chain derivatives, for which the molecular biophysical properties and interactions with membrane lipids are even less known than those of Cer). However, as in most membrane-related studies, fundamental features of the molecular and topological behavior of natural membranes can be subsequently explained on the basis of phenomena understood first in molecular terms using well-defined and controlled model membrane systems.

If the effects of natural Cer as a signaling lipid mediator have any influence on the biophysical properties of cell membranes, those will have to be confined, at least initially, to its site of metabolic production in the plasma membrane or intracellular membranes. Moreover, similar to all other known effects of lipid mediators (1) and other sphingolipid biomodulators (13), the influence on membrane organization will be first exerted restricted to a membrane region of mesoscopic size where the lipid is concentrated by transient dynamic clustering or by metabolism. Studies on membrane composition and asymmetry for defined cell types in culture are still very scarce and most speculations usually rely on data from a handful of simple membrane types. Conclusions obtained from the accessibility of some membranes of specific cells to lipid degradation by bacterial sphingomyelinase have identified different pools of sphingomyelin in the plasma membrane and intracellular membrane vesicles (44, 45). The sphingomyelin pool that undergoes significant hydrolysis in response to biological inducers of the sphingomyelin cycle related to cell regulatory functions is mostly located at the inner leaflet of the plasma membrane, or at the cytoplasmic face of subcellular vesicles (44). In many of the cellular effects, sphingomyelin degradation and increases of Cer levels are transient but rather slow processes, in molecular terms, that may last from minutes to hours (46–48) and during which fast events related to molecular interactions, domain formation, and changes of membrane topology of the type described by us and other authors can take place (5, 7, 14, 17, 19, 20, 25). Thus, when the physiological response is observed, this is the reflection of several combined changes of the structure and dynamics of the membrane of the type described above. It is also relevant to compare the proportions of Cer at which the molecular changes take place in relation to those occurring during the biological effects. It should be emphasized that in the few cases in which they have been analytically measured, and contrary to some common assumptions, the variation of the endogenous basal levels of these sphingolipids during cell stimulation are by no means negligible. For example, exposure of monoblastic leukemia cells to tumor necrosis factor (TNF-α) causes about 30% sphin-

gomyelin hydrolysis and increases of Cer from about 28 pmol/nmol P_i to 40 pmol/nmol P_i in 10 min (47). The response of Fas-sensitive cells to an agonist monoclonal antibody induced 2- to 3-fold increases of the activity of a membrane-bound Mg-dependent sphingomyelinase leading to 21% decrease of the sphingomyelin mass and an increase of the basal level of Cer from about 6 pmol/nmol P_i to more than 13 pmol/nmol P_i in 8 h (46). Treatment of leukemia cell lines with a chemotherapeutic agent that induces apoptosis also caused about 25% hydrolysis of sphingomyelin by a neutral membrane sphingomyelinase in about 8 min, with the concomitant increase of the basal level of intracellular Cer by about 30% (48).

When expressed in terms comparative to those used in our biophysical experiments, the figures obtained in the biological studies represent changes in the proportions of Cer that amount to between 3 to 10 mole % with respect to phosphatidylcholine (whose content in different biomembranes is about 40–50% of the total P_i). Obviously, local concentrations or relative proportions in laterally segregated domains or at the site of metabolic production will be considerably higher and on the basis of our experiments it should be expected that the very increase in the proportions of Cer in the range observed in the biological studies or even below (1 to 4 mole %, see Figs. 1A and B) should induce considerable changes in the phospholipid phase behavior, molecular packing, dipole potential, and local demixing with formation of Cer-enriched domains.

Alterations by Cer of the molecular packing properties of other natural phospholipids and glycosphingolipids were reported by our laboratory more than 20 years ago (for references see 14) and Cer-induced phase changes have been described for other phospholipids and some more complex mixtures (7, 8, 24, 49). In turn, the changes in the relative proportions of sphingomyelin, Cer, and phospholipid should have amplified responses on the membrane dynamics and metabolism. We and others have previously shown evidences on the molecular cross-communication and the intermolecular packing-dependent mutual regulation of the sphingomyelin and phosphatidylcholine degradative pathways mediated by sphingomyelinase and phospholipase A_2 (22–24) and phospholipase C (7). Also, mutually regulated effects of sphingomyelinase and phospholipase C participate in mediating vesicle membrane fusion (7), probably through a balanced effect of diacylglycerol and Cer in promoting formation of non-bilayer phases (25) that is a topological requirement for complete lipid bilayer fusion (6, 20). In close relation to the aspects of membrane recombination and fusion involving non-bilayer phases or phase separation processes possibly induced by Cer, it is also worth mentioning that valuable insights into the question of vesicle membrane traffic in animal cells are frequently obtained using fluorescent Cer analogs as vital stains for the Golgi apparatus. One of these probes (a short-chain ceramide derivative: C_5-dimethyl-BODIPY-Cer) exhibits a spectral change that allows visualization of green or red fluorescence depending on its relative proportions in the vesicle membranes in their way to the plasma membrane (50). In relation to our experiments, it is interesting that the observed spectral shift in the Golgi vesicles indicates that the Cer analog and its metabolically generated sphingomyelin derivative (which in cell biology studies are frequently taken implicitly as likely reporters for the behavior of the natural lipids) are present in proportions of more than 5 mole % with respect to the phospholipid (50). Again, this is well within the range of concentration at which Cer induces the biological effects in cellular systems and the alterations of membrane organization described in our work.

The different data, obtained by means of calorimetry, monolayers, and cluster distribution function analysis discussed in this work under well-defined control of molecular packing, surface electrostatics, and thermodynamic properties, are in keeping with each other and provide a consistent insight of the possible molecular effects of natural Cer in biomembranes. It has been shown (25) that natural Cer in mixtures with dePE has the effect of increasing the gel–fluid midpoint transition temperature by ~8°C, similar to our system containing dpPC. It was also shown that endotherms were asymmetric, revealing the existence of several components, and ^{31}P NMR demonstrated that Cer also facilitated inverted hexagonal phase formation.

The phase diagram (Fig. 2) describing the variation of T_S with the proportion of Cer in the system, with the existence of partial two-gel phase immiscibility at small proportions of the sphingolipid, resembles phase diagrams typically obtained for lipids exhibiting relatively large hydrocarbon chain mismatch; the gel phase immiscibility in these bilayer membranes has been interpreted on the basis of the existence of different possibilities for various types of chain interdigitation (24, 51). In mixtures of dmPC with a natural Cer fraction containing hydrocarbon chains with a considerable proportion of hydroxylated fatty acids, it was suggested that Cer-enriched phases were present above 10 mole % Cer, occurring with segregation of a fluorescent lipid probe into microdomains (49). Although a partial phase diagram was not reported by these authors, their calorimetry data indicate that Cer induced a decrease of the melting temperature of dmPC above a mole fraction of Cer of 0.1; also, DPH depolarization suggested a certain degree of immiscibility of two types of gel phases in mixtures with dmPC below 20°C while a miscible behavior was observed at 30°C (which is above the T_m of dmPC) in all systems containing Cer up to 30 mole % (49). These authors considered that the formation of the segregated probe's microdomains could be explained by the effect of Cer-induced phase separation due to hydrophobic mismatch between the long-chain natural ceramides and dmPC. Also, mixtures of dmPC and C24-sphingomyelin (having considerable chain mismatch) shows phase separation of pure dmPC while this phospholipid is fully miscible with C16-sphingomyelin that contains hydrocarbon chains of equal length (52). As a first step in our studies, a natural mixture of non-hydroxylated Cer was used. The high percentage of long chain fatty acids contained in this fraction implies the existence of possibilities for average chain mismatch and interdigitation that could occur

both between molecules of Cer and with dpPC. Whether the segregated phases enriched in Cer described in our work are constituted by defined molecular species of Cer, and which of these may have a greater effect on the alteration of the phospholipid packing and thermodynamic properties, will require additional prolonged studies in more detail.

The cluster distribution functions derived from the calorimetry experiments coincide in defining three regions that show distinct thermodynamically correlated behavior. The cluster analysis reveals that the different coexisting component transitions have different individual cluster distribution function parameters, which indicates that Cer induces a high degree of domain microheterogeneity besides introducing phase heterogeneity and immiscibility in the system. The average cluster size, densities, and fraction of lipid at the gel–liquid crystalline boundary for each component transition change markedly over critical ranges of composition but exhibit generally similar characteristics within each range. These ranges of composition correspond to systems containing less than 8 mole % Cer, between 8 and 20 mole % Cer, above 20 mole % Cer, which are approximately the proportions over which defined laterally segregated phases S_1, S_2, and S_3 are present.

Dipole potentials can be major determinants for the surface distribution of microheterogeneous domains in lipid monolayers (53) and differences in the degree of molecular polarization and dipole potential are directly responsible for determining the size, shape, and arrangement of lipid domains as observed by fluorescence microscopy (54). The hyperpolarization seen at 24°C in the monolayer studies suggests that unfavorable dipolar matching (with energetically demanding hyperpolarization) between molecules of Cer and dpPC can be at least one of the probable local molecular determinants for the lateral segregation of Cer from dpPC in the condensed gel phase as described in the calorimetry studies.

This work was supported in part by SECyT-UNC, CONICOR, FONCyT, and CONICET, Argentina. D.C.C is a postgraduate fellow and B.M is Principal Career Investigator of CONICET.

Manuscript received 8 March 1999 and in revised form 28 May 1999.

REFERENCES

1. Exton, J. H. 1990. Signaling through phosphatidylcholine breakdown. *J. Biol. Chem.* **265:** 1–4.
2. Spiegel, S., O. Cuvillier, L. C. Edsall, T. Kohama, R. Menzeleev, A. Olah, A. Olivera, G. Pirianov, D. M. Thomas, Z. Tu, J. R. van Brocklyn, and F. Wang. 1998. Sphingosine-1-phosphate in cell growth and cell death. *Ann. NY Acad. Sci.* **845:** 11–18.
3. Hannun, Y. A., and R. M. Bell. 1989. Functions of sphingolipids and sphingolipid breakdown products in cellular regulation. *Science.* **243:** 500–507.
4. Kolesnick, R. N. 1991. Sphingomyelin and derivatives as cellular signals. *Prog. Lipid Res.* **30:** 1–38.
5. Jimenez-Monreal, A. M., J. Villalain, F. J. Aranda, and J. C. Gomez-Fernandez. 1998. The phase behavior of aqueous dispersions of unsaturated mixtures of diacylglycerols and phospholipids. *Biochim. Biophys. Acta.* **1373:** 209–219.
6. Seddon, J. M., and R. H. Templer.1993. Cubic phases of self-assembled amphiphilic aggregates. *Phil. Trans. R. Soc. Lond. A.* **344:** 377–401.
7. Begoña Ruiz-Argüello, M., F. M. Goñi, and A. Alonso. 1998. Vesicle membrane fusion induced by the concerted activities of sphingomyelinase and phospholipase C. *J. Biol. Chem.* **273:** 22977–22982.
8. Huang, H. W., E. M. Goldberg, and R. Zidovetzki. 1996. Ceramide induces structural defects in phosphatidylcholine bilayers and activates phospholipase A_2. *Biochem. Biophys. Res. Commun.* **220:** 834–838.
9. Ransac, S., H. Moreau, C. Riviere, and R. Verger. 1991. Monolayer techniques for studying phospholipase kinetics. *Methods Enzymol.* **197:** 49–65.
10. Bell, J. D., and R. L. Biltonen. 1991. Activation of phospholipase A_2 on lipid bilayers. *Methods Enzymol.* **197:** 249–258.
11. Jain, M. K., and O. G. Berg. 1989.The kinetics of interfacial catalysis by PLA_2 and regulation of interfacial activation: hopping versus scooting. *Biochim. Biophys. Acta.* **1002:** 127–156.
12. Yu, R. K., and M. Saito. 1989. Structure and localization of gangliosides. *In* Neurobiology of Glycoconjugates. R. V. Margolis and R. K. Margolis, editors. Plenum Press, New York. 1–42.
13. Hakomori, S. 1990. Bifunctional role of glycosphingolipids. Modulations for transmembrane signaling and mediators for cellular interactions. *J. Biol. Chem.* **265:** 18713–18716.
14. Maggio, B. 1994. The surface behaviour of glycosphingolipids in biomembranes: a new frontier in molecular ecology. *Prog. Biophys. Mol. Biol.* **62:** 55–117.
15. Maggio, B., T. Ariga, J. M. Sturtevant, and R. K. Yu. 1985. Thermotropic behavior of binary mixtures of dipalmitoylphosphatidylcholine and glycosphingolipids in aqueous dispersions. *Biochim. Biophys. Acta.* **818:** 1–12.
16. McLaughlin, S. M. 1989. The electrostatic properties of membranes. *Annu. Rev. Biophys. Biophys. Chem.* **18:** 113–136.
17. Perillo, M. A., N. J. Scarsdale, R. K. Yu, and B. Maggio. 1994. Modulation by gangliosides of the lamellar-inverted micelle (hexagonal II) phase transition in mixtures containing phosphatidylethanolamine and dioleoylglycerol. *Proc. Natl. Acad. Sci. USA.* **91:** 10019–10023.
18. van Gorkom, L. C. M., J. J. Cheetham, and R. M. Epand. 1995. Ganglioside GD1a generates domains of high curvature in phosphatidylethanolamine liposomes as determined by solid state ^{31}P-NMR spectroscopy. *Chem. Phys. Lipids.* **76:** 103–108.
19. Maggio, B., and R. K. Yu. 1992. Modulation by glycosphingolipids of membrane-membrane interactions induced by myelin basic protein and melittin. *Biochim. Biophys. Acta.* **112:** 105–114.
20. Basañez, G., G. D. Fidelio, F. M. Goñi, B. Maggio, and A. Alonso. 1996. Dual inhibition effect of gangliosides on phospholipase C—promoted fusion of lipid vesicles. *Biochemistry.* **35:** 7506–7513.
21. Maggio, B., I. D. Bianco, G. G. Montich, G. D. Fidelio, and R. K. Yu. 1994. Regulation by gangliosides and sulfatides of phospholipase A_2 activity against dipalmitoyl- and dilauroylphosphatidylcholine in small unilamellar bilayer vesicles and mixed monolayers. *Biochim. Biophys. Acta.* **1190:** 137–148.
22. Fanani, M. L., and B. Maggio. 1997. Mutual modulation of sphingomyelinase and phospholipase A_2 activities against mixed lipid monolayers by their lipid intermediates and glycosphingolipids. *Mol. Membr. Biol.* **14:** 25–29.
23. Fanani, M. L., and B. Maggio. 1998. Surface pressure—dependent cross-modulation of sphingomyelinase and phospholipase A_2 in monolayers. *Lipids.* **33:** 1079–1087.
24. Huang, H., E. M. Goldberg, and R. Zidovetzki. 1998. Ceramides perturb the structure of phosphatidylcholine bilayers and modulate the activity of phospholipase A_2. *Eur. Biophys. J.* **27:** 361–366.
25. Veiga, M. P., J. L. R. Arrondo, F. M. Goñi, and A. Alonso. 1999. Ceramides in phospholipid membranes: effects on bilayer stability and transition to nonlamellar phases. *Biophys. J.* **76:** 342–350.
26. Levade, T., M-C. Tempesta, and R. Salvayre. 1993. The in situ degradation of ceramide, a potential lipid mediator, is not completely impaired in Farber disease. *FEBS Lett.* **329:** 306–312.
27. Freire, E., and R. Biltonen.1978. Estimation of molecular averages and equilibrium fluctuations in lipid bilayer systems from the excess heat capacity function. *Biochim. Biophys. Acta.* **514:** 54–68.
28. Bianco, I. D., G. D. Fidelio, and B. Maggio. 1988. Effect of glycerol on the molecular properties of cerebrosides, sulphatides and gangliosides in monolayers. *Biochem. J.* **251:** 613–616.
29. Maggio, B., T. Ariga, J. M. Sturtevant, and R. K. Yu. 1985. Thermo-

tropic behavior of glycosphingolipids in aqueous dispersions. *Biochemistry.* **24:** 1084–1092.
30. Wertz, P. W., W. Abraham, L. Landmann, and D. T. Downing. 1986. Preparation of liposomes from stratum corneum lipids. *J. Invest. Dermatol.* **87:** 582–584.
31. Fidelio, G. D., B. Maggio, and F. A. Cumar. 1986. Molecular parameters and physical state of neutral glycosphingolipids and gangliosides in monolayers at different temperatures. *Biochim. Biophys. Acta.* **854:** 231–239.
32. Wartewig, S., R. Neubert, W. Rettig, and K. Hesse. 1997. Structure of stratum corneum lipids characterized by FT-Raman spectroscopy and DSC. IV. Mixtures of ceramides and oleic acid. *Chem. Phys. Lipids.* **91:** 145–152.
33. Shah, J., J. M. Atienza, A. V. Rawlings, and G. G. Shipley. 1995. Physical properties of ceramides: effect of fatty acid hydroxylation. *J. Lipid Res.* **36:** 1945–1955.
34. Lofgren, H., and I. Pascher. 1977. Molecular arrangements of sphingolipids. The monolayer behaviour of ceramides. *Chem. Phys. Lipids.* **20:** 273–284.
35. Mabrey, S., and J. M. Sturtevant. 1976. Investigation of phase transitions of lipids and lipid mixtures by high sensitivity differential scanning calorimetry. *Proc. Natl. Acad. Sci. USA.* **73:** 3862–3866.
36. Biltonen, R. L. 1990. A statistical thermodynamic view of cooperative structural changes in phospholipid bilayer membranes. *J. Chem. Thermodynamics.* **22:** 1–19.
37. Nagle, J. F. 1986. Theory of lipid monolayer and bilayer chain-melting phase transitions. *Faraday Discuss. Chem. Soc.* **81:** 151–162.
38. Mondat, M., A. Georgallas, D. A. Pink, and M. J. Zuckermann. 1984. The thermodynamic properties of mixed phospholipid bilayers: a theoretical analysis, *Can. J. Biochem. Cell Biol.* **62:** 796–802.
39. Marcelja, S., and J. Wolfe. 1979. Properties of bilayer membranes in the phase transition or phase separation region. *Biochim. Biophys. Acta.* **557:** 24–31.
40. Maggio, B., F. A. Cumar, and R. Caputto. 1978. Surface behavior of gangliosides and related glycosphingolipids. *Biochem. J.* **171:** 1113–1118.
41. Sears, D. F., and R. E. Stark. 1973. Biological Horizons in Surface Science. Academic Press, New York. 1–33.
42. Baret, J. F., H. Hasmonay, J. L. Firpo, J. J. Dupin, and M. Dupeyrat. 1982. The different types of isotherm exhibited by insoluble fatty acid monolayers. A theoretical interpretation of phase transitions in the condensed state. *Chem. Phys. Lipids.* **30:** 177–187.
43. Maggio, B., and J. A. Lucy. 1976. Polar group behaviour in mixed monolayers of phospholipids and fusogenic lipids. *Biochem. J.* **155:** 353–364.
44. Linardic, C. M., and Y. A. Hannun. 1994. Identification of a distinct pool of sphingomyelin involved in the sphingomyelin cycle. *J. Biol. Chem.* **269:** 23530–23537.
45. Calderon, R. O., and G. N. DeVries. 1997. Lipid composition and phospholipid asymmetry of membranes from a Schwann cell line. *J. Neurosci. Res.* **49:** 372–380.
46. Tepper, C. G., S. Jayadev, B. Liu, A. Bielawska, R. Wolff, S. Yonehara, Y. A. Hannun, and M. F. Seldin. 1995. Role for ceramide as an endogenous mediator of Fas-induced cytotoxicity. *Proc. Natl. Acad. Sci. USA.* **92:** 8443–8447.
47. Obeid, L. M., C. M. Linardic, L. A. Karolak, and Y. A. Hannun. 1993. Programmed cell death induced by ceramide. *Science.* **259:** 1769–1771.
48. Jaffrézou, J-P., T. Levade, A. Bettaïeb, N. Andrieu, C. Bezombes, N. Maestre, S. Vermeersch, A. Rousse, and G. Laurent. 1996. Daunorubicin—induced apoptosis: triggering of ceramide generation through sphingomyelin hydrolisis. *EMBO J.* **15:** 2417–2424.
49. Holopainen, J. M., J. Y. A. Lehtonen, and P. K. I. Kinnunen. 1997. Lipid microdomains in dimiristoylphosphatidylcholine—ceramide liposomes. *Chem. Phys. Lipids.* **88:** 1–13.
50. Pagano, R. E., O. C. Martin, H. C. Kang, and R. P. Haugland. 1991. A novel fluorescent ceramide analogue for studying membrane traffic in animal cells: accumulation at the Golgi apparatus results in altered spectral properties of the sphingolipid precursor. *J. Cell Biol.* **113:** 1267–1279.
51. Mason, J. T. 1988. Mixing behavior of symmetric chain length and mixed chain length phosphatidylcholines in two-component multilamellar bilayers: Evidence for gel and liquid-crystalline phase immiscibility. *Biochemistry.* **27:** 4421–4429.
52. Bar, L. K., Y. Barenholz, and T. E. Thompson. 1997. Effect of sphingomyelin composition on the phase structure of phosphatidylcholine—sphingomyelin bilayers. *Biochemistry.* **36:** 2507–2516.
53. Brockman, H. 1994. Dipole potential of lipid membranes. *Chem. Phys. Lipids* .**73:** 57–79.
54. Möhwald, H. 1990. Phospholipid and phospholipid-protein monolayers at the air/water interface. *Annu. Rev. Phys. Chem.* **41:** 441–476.